Supporting Information

Extremely High-Efficiency Solar Steam Generation, Robust and Scalable Photothermal Evaporator Based on ZIF-67@MXene/rGO Decorated on Rock Wool

Riski Titian Ginting[a,b], Hairus Abdullah[c], Diana Alemin Barus[d], Vivi Fauzia[e]

[a]Department of Electrical Engineering, Universitas Prima Indonesia, Medan, Indonesia

[b]Nanomaterials for Renewable Energy Laboratory, CV. Inovasi Teknologi Nano, Medan, Indonesia

[c]Department of Industrial Engineering, Universitas Prima Indonesia, Medan, Indonesia

[d]Department of Physics, Faculty of Mathematics and Natural Sciences, Universitas Sumatera Utara, Medan, Indonesia

[e]Department of Physics, Faculty of Mathematics and Natural Sciences, Universitas Indonesia, Depok, Indonesia

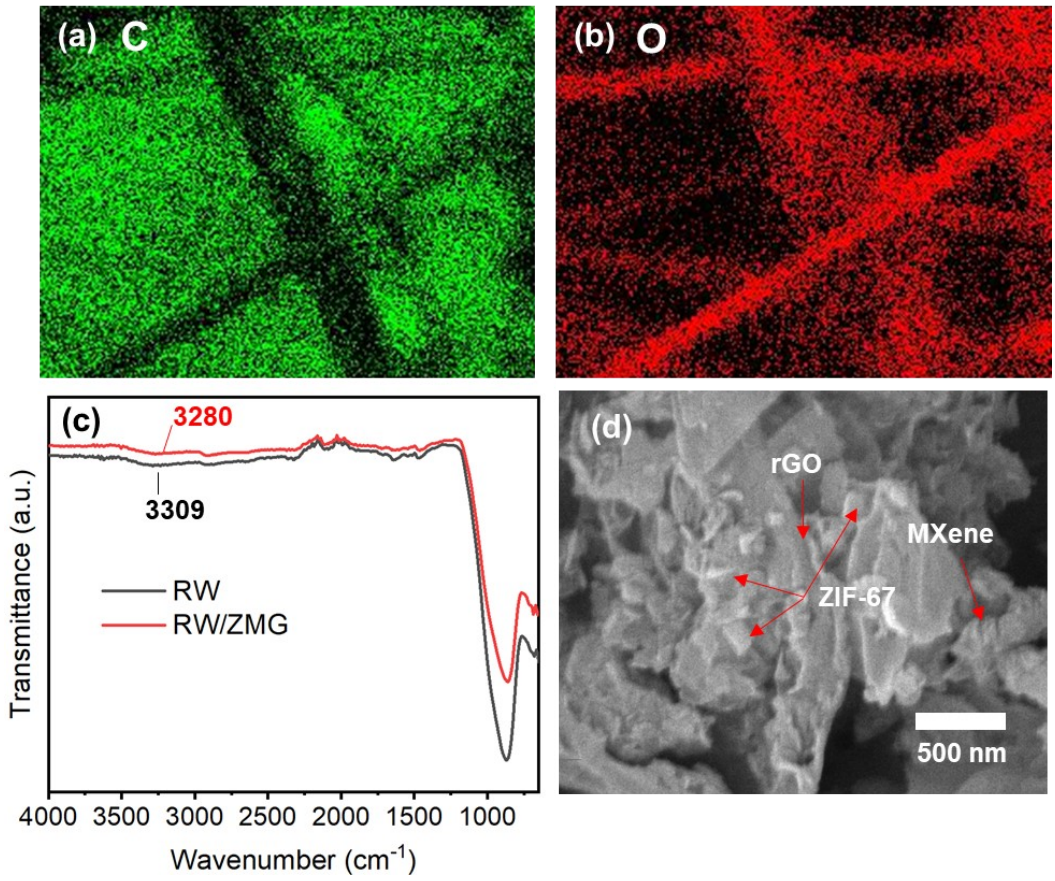

Fig. S1. EDX elemental mapping of (a) C and (b) O for RW/ZMG sample. (c) FTIR spectra of RW and RW/ZMG sample. (d) SEM image of ZMG sample (Red arrow indicates the existence of ZIF-67, MXene and rGO).

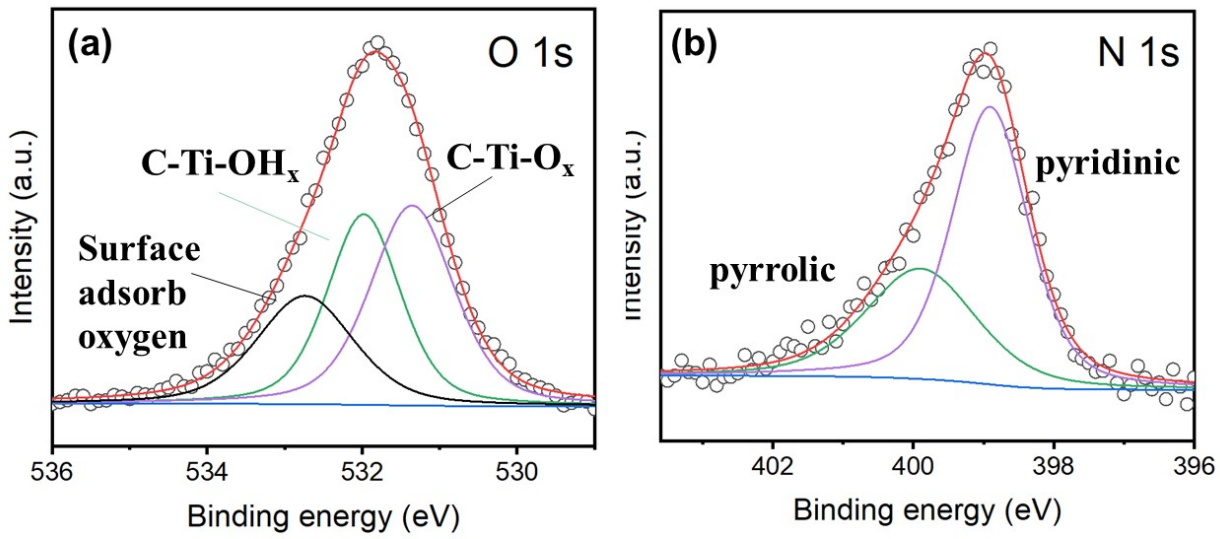

Fig. S2 Narrow scan XPS of (a) O 1s and (b) N 1s of RW/ZMG sample.

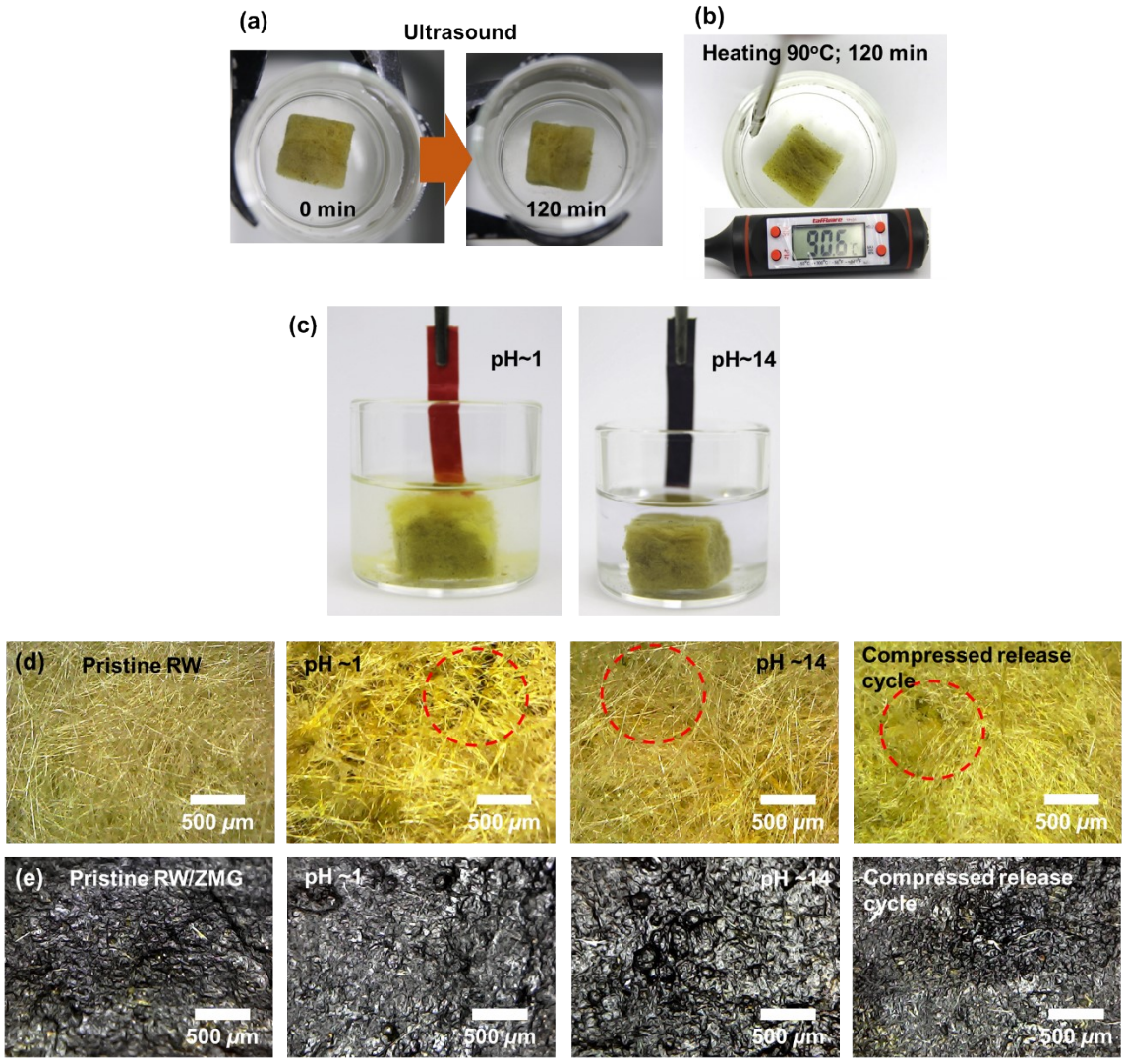

Fig. S3 (a) Photograph of RW waste sample under harsh condition of (a) ultrasound for 120 min, (b) heating at 90°C for 120 min, and (c) pH effect. Microscopic images of (d) RW and (e) RW/ZMG sample before and after immersed in pH~1 & 14 and after compressed released cycle.

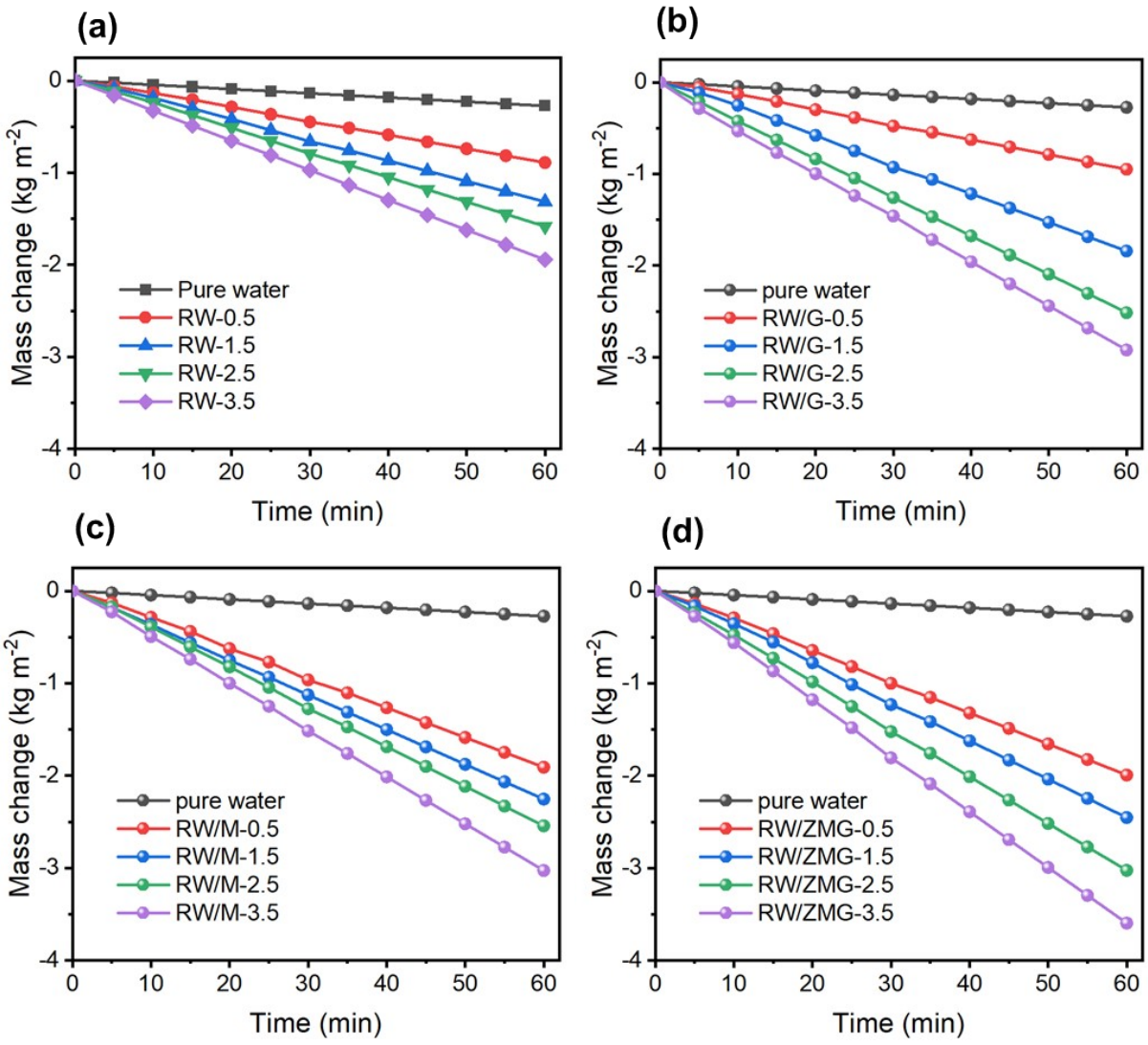

Fig. S4. Mass change as a function of time with various height 0.5, 1.5, 2.5 and 3.5 cm for (a) RW, (b) RW/G, (c) RW/M and (d) RW/ZMG under 1 sun illumination.

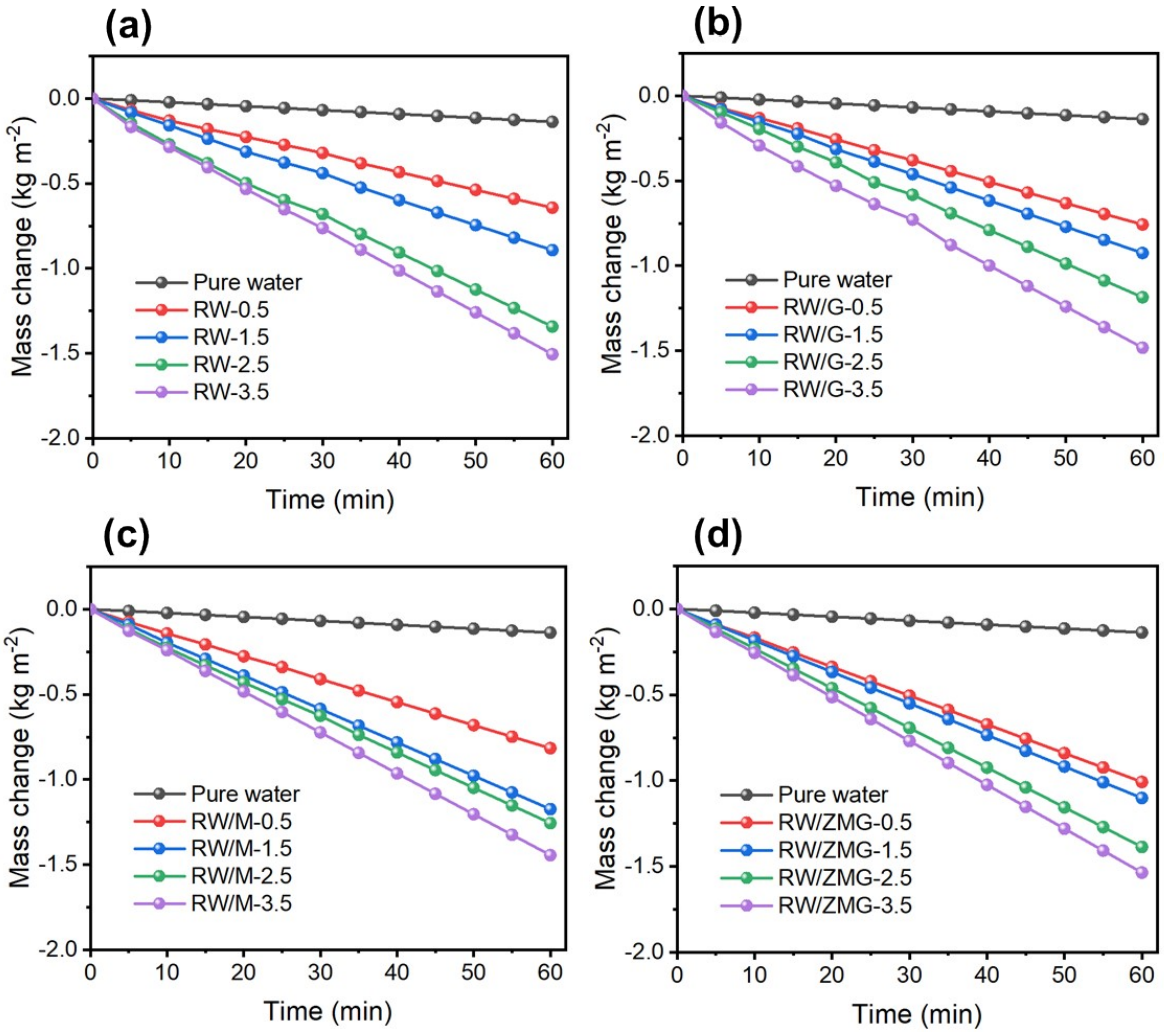

Fig. S5. Mass change as a function of time with various height 0.5, 1.5, 2.5 and 3.5 cm for (a) RW, (b) RW/G, (c) RW/M and (d) RW/ZMG under dark condition.

Table S1. Summarized evaporation rate and efficiency of pristine and functionalized RW sample.

Sample	Height (cm)	Evaporation rate (kg m^{-2} h^{-1})	Evaporation Efficiency (%)	Net environment energy (W)*
RW	0.5	0.88	16.4	-
	1.5	1.31	25.6	-0.112
	2.5	1.58	27.3	-0.166
	3.5	1.94	29.7	-0.158
RW/G	0.5	0.95	40.7	-
	1.5	1.84	62.8	0.0078
	2.5	2.51	91.0	0.064
	3.5	2.92	98.5	0.11
RW/M	0.5	1.91	64.7	-
	1.5	2.25	74.4	0.009
	2.5	2.54	88.0	0.036
	3.5	3.03	107.9	0.05
RW/GMZ	0.5	1.99	67.9	-
	1.5	2.45	92.4	0.02
	2.5	3.02	112.2	0.07
	3.5	3.78	153.7	0.128

*Side evaporator area are 1.5, 2.5 and 3.5 cm are 12, 20 and 28 cm^2, respectively.

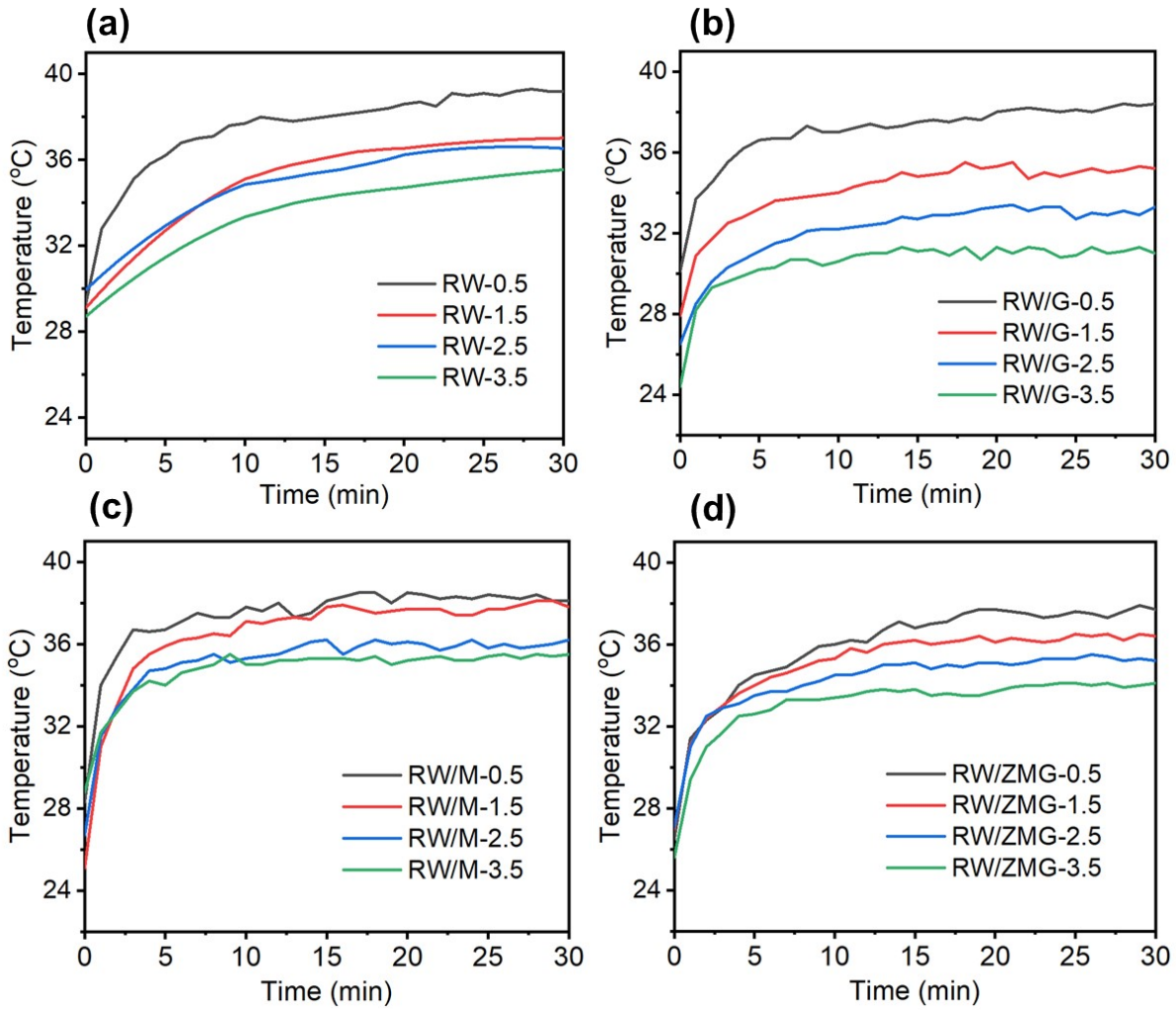

Fig. S6. Time-dependent evaporation temperature profile of top surface with various height 0.5, 1.5, 2.5 and 3.5 cm for (a) RW, (b) RW/G, (c) RW/M and (d) RW/ZMG under 1 sun illumination.

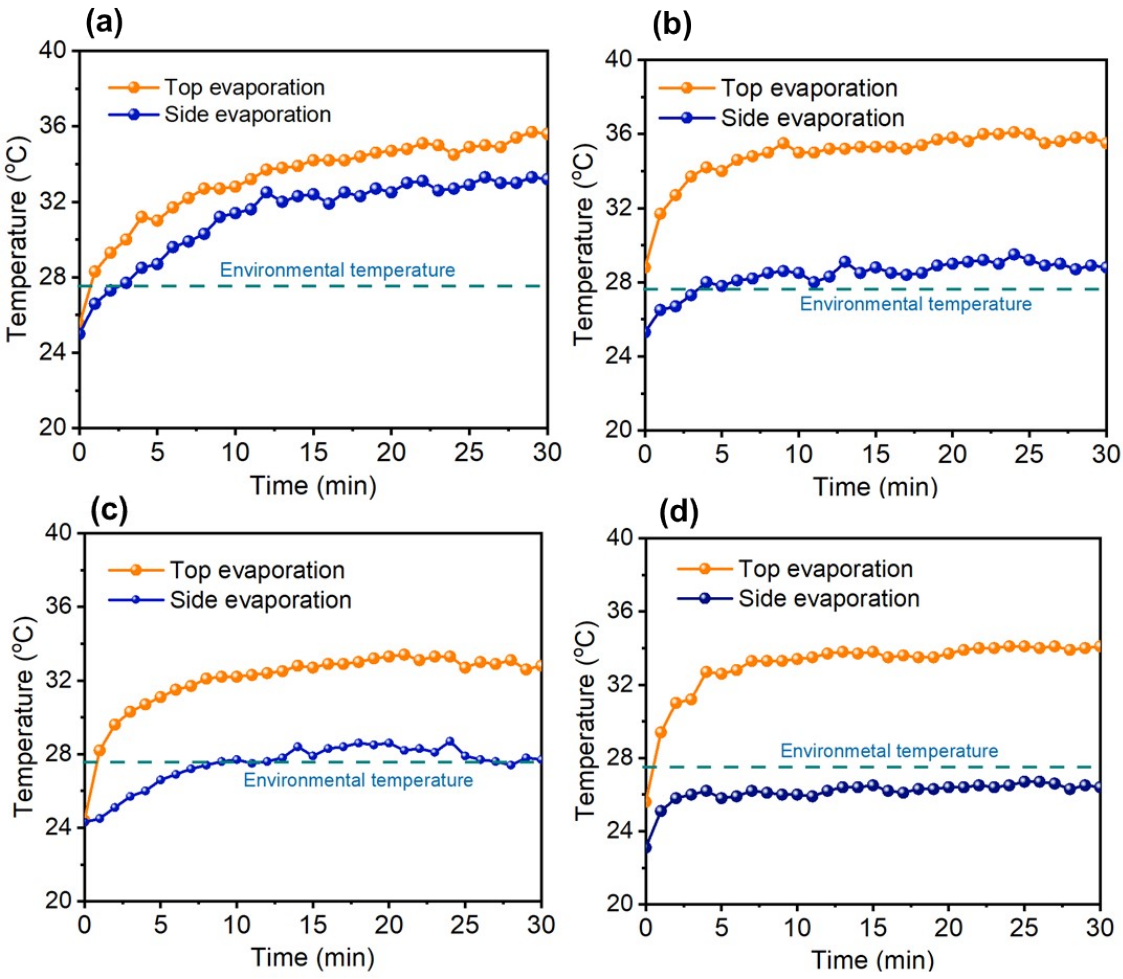

Fig. S7. Time-dependent evaporation temperature profile of top and side surface with height of 3.5 cm for (a) RW, (b) RW/G, (c) RW/M and (d) RW/ZMG under 1 sun illumination.

.

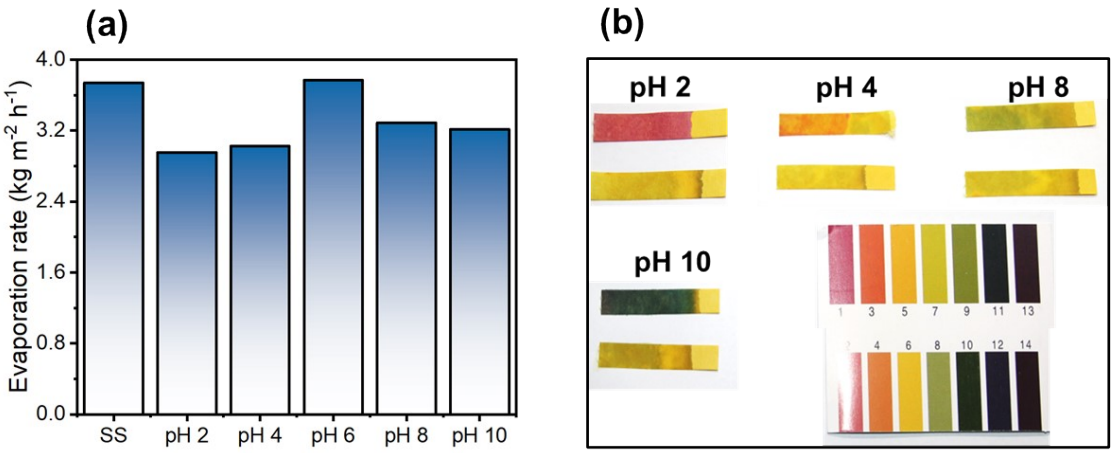

Fig. S8. (a) Evaporation rate of RW/ZMG with different conditions under 1 sun irradiation. (b) pH paper before and after condensed water collected with RW/ZMG evaporator.

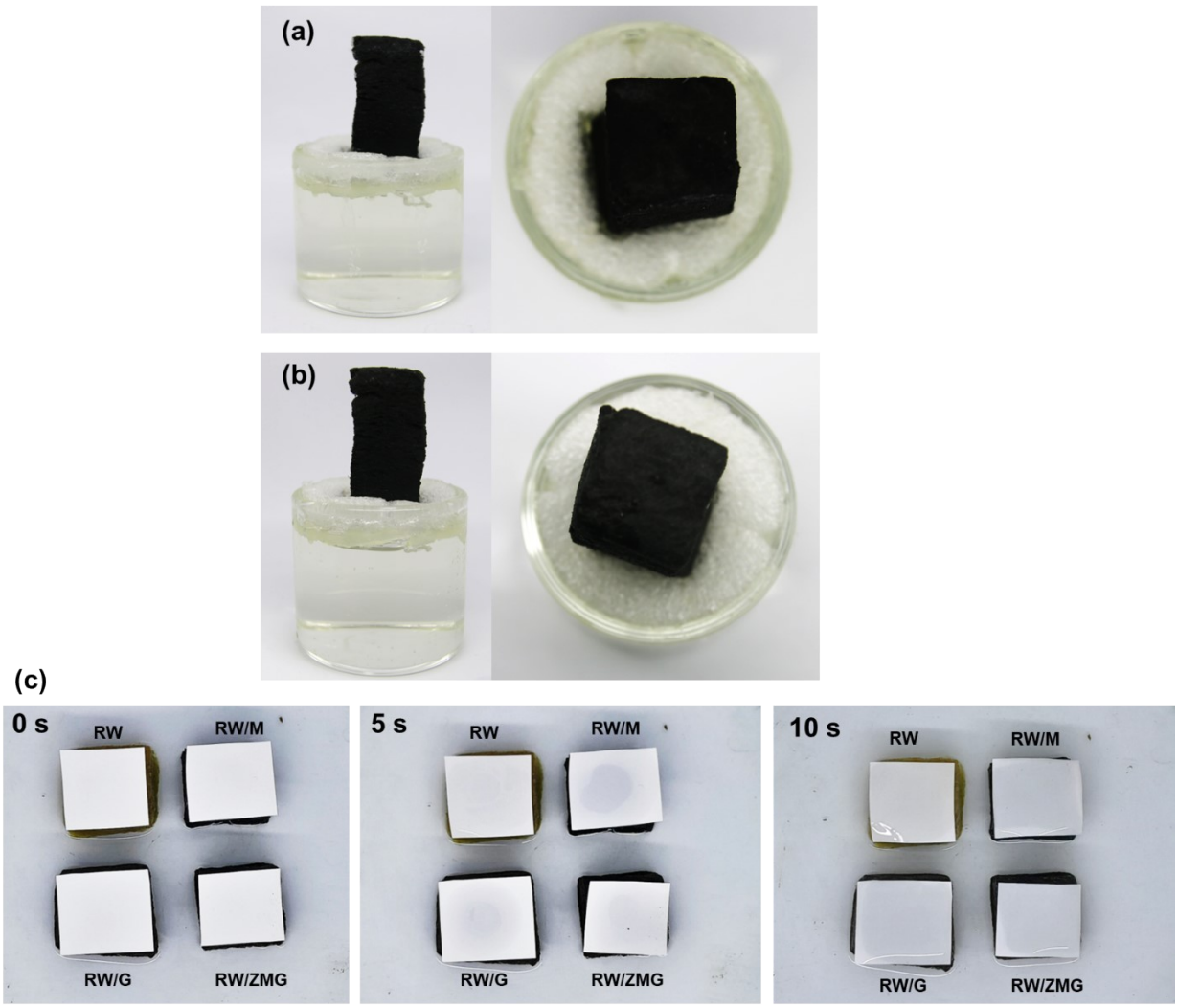

Fig. S9. Photograph image of RW/ZMG evaporator in 200mL of 20 wt% NaCl under 1 sun illumination of (a) before and (b) without any salt crystals after 12 h. (c) Photograph image of wetting process of with methyl cellulose ester (MCE) membrane on top of RW, RW/G, RW/M and RW/ZMG sample.

Table S2. Summarized of evaporation rate and efficiency from previous reported results in comparison with current work.

Evaporator materials	Height (cm)	Evaporation rate (kg m^{-2} h^{-1})	Evaporation efficiency (%)	Ref.
Polyester fiber bundles /polypyrrole	6	3.77	155.77	[1]
Cellulose acetate fiber /MXene	2	1.82	80.2	[2]
	4	2.42	97.3	
	6	3.38	132.9	
Polydopamine (PDA)-functionalized cellulose aerogels	3	2.74	96.5	[3]
PP hollow fiber membrane/dopamine	0.5	2.6	115.14	[4]
Polydopamine coated nickel-cobalt bimetal (Ni_1Co_3@PDA) nanosheets	6	2.42	109	[5]
Cotton sheet/rGO-agarose	15	4	133	[6]
Sweet potato starch/squid ink	0.5	2.07	93.7	[7]
	2	2.3	98.4	
	5	2.62	108.1	
CuS-cellulose nanofiber	9	3.94	162.7	[8]
Setaria viridis spike / Ppy	6	3.72	92.1	[9]
Carbon fiber bundles	2	1.94	99.95	[10]
	4	2.48	111.14	
	6	2.99	120.15	
N-doped carbon@Cu (NC@Cu) core–shell nanostructure	0.5	1.71	96.8	[11]
	2	2.04	116.3	

	4	2.37	117.6	
	6	2.76	137.1	
Natural corn straw cavity structure with polyurethane sponge	6	2.18	93.5	[12]
RW	0.5	0.88	16.4	
	1.5	1.31	25.6	This
	2.5	1.58	27.3	work
	3.5	1.94	29.7	
RW/G	0.5	0.95	40.7	
	1.5	1.84	62.8	This
	2.5	2.51	91.0	work
	3.5	2.92	98.5	
RW/M	0.5	1.91	64.7	
	1.5	2.25	74.4	This
	2.5	2.54	88.0	work
	3.5	3.03	107.9	
RW/ZMG	0.5	1.99	67.9	
	1.5	2.45	92.4	This
	2.5	3.02	112.2	work
	3.5	**3.81**	**153.7**	

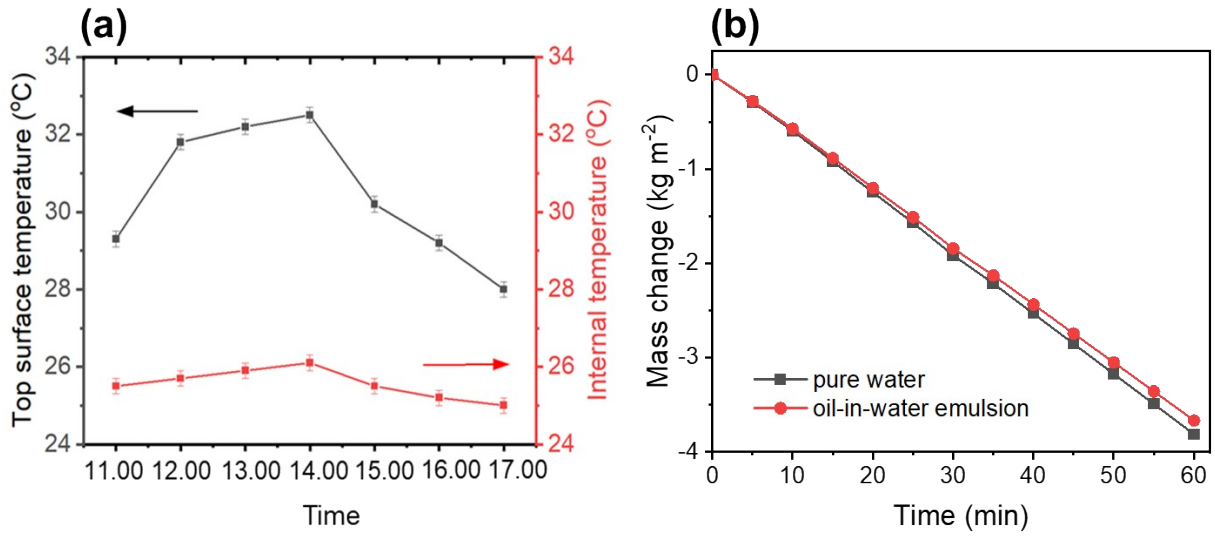

Figure S10. (a) Top surface and internal temperature of RW/ZMG evaporator deployed for outdoor experiments. (b) Mass change against time for RW/ZMG evaporator of pure water and oil-in-water emulsion.

References

[1] J. Xiong, J. Yi, S. Peng, Z. Yang, Y. Wu, W. Wang, S. Lv, J. Peng, C. Xue, X. Min, Plant transpiration-inspired environmental energy-enhanced solar evaporator fabricated by polypyrrole decorated polyester fiber bundles for efficient water purification, Journal of Cleaner Production, (2022) 134683.

[2] W. Li, X. Tian, X. Li, J. Liu, C. Li, X. Feng, C. Shu, Z.-Z. Yu, An environmental energy-enhanced solar steam evaporator derived from MXene-decorated cellulose acetate cigarette filter with ultrahigh solar steam generation efficiency, Journal of Colloid and Interface Science, 606 (2022) 748-757.

[3] H. Liu, M.K. Alam, M. He, Y. Liu, L. Wang, X. Qin, J. Yu, Sustainable cellulose aerogel from waste cotton fabric for high-Performance solar steam generation, ACS Applied Materials & Interfaces, 13 (2021) 49860-49867.

[4] C. Wei, X. Zhang, S. Ma, C. Zhang, Y. Li, D. Chen, H. Jiang, Z. Xu, X. Huang, Ultra-robust vertically aligned three-dimensional (3D) Janus hollow fiber membranes for interfacial solar-

driven steam generation with salt-resistant and multi-media purification, Chemical Engineering Journal, 425 (2021) 130118.

[5] B. Shao, Y. Wang, X. Wu, Y. Lu, X. Yang, G.Y. Chen, G. Owens, H. Xu, Stackable nickel–cobalt@ polydopamine nanosheet based photothermal sponges for highly efficient solar steam generation, Journal of Materials Chemistry A, 8 (2020) 11665-11673.

[6] X. Wu, T. Gao, C. Han, J. Xu, G. Owens, H. Xu, A photothermal reservoir for highly efficient solar steam generation without bulk water, Science Bulletin, 64 (2019) 1625-1633.

[7] Y. Xu, X. Xiao, X. Fan, Y. Yang, C. Song, Y. Fan, Y. Liu, Low cost, facile, environmentally friendly all biomass-based squid ink-starch hydrogel for efficient solar-steam generation, Journal of Materials Chemistry A, 8 (2020) 24108-24116.

[8] Y. Chen, Y. Wang, J. Xu, M.R. Ibn Raihan, B. Guo, G. Yang, M. Li, H. Bao, H. Xu, A 3D Opened Hollow Photothermal Evaporator for Highly Efficient Solar Steam Generation, Solar RRL, (2022) 2200202.

[9] Z. Xie, J. Zhu, L. Zhang, Three-dimensionally structured polypyrrole-coated setaria viridis spike composites for efficient solar steam generation, ACS Applied Materials & Interfaces, 13 (2021) 9027-9035.

[10] G. Zhao, Y. Chen, L. Pan, B. Chen, L. Ren, X. Xiao, H. Yang, W. Xu, Plant-inspired design from carbon fiber toward high-performance salt-resistant solar interfacial evaporation, Solar Energy, 233 (2022) 134-141.

[11] F. Meng, Z. Ding, Z. Chen, K. Wang, X. Liu, J. Li, T. Lu, X. Xu, L. Pan, N-doped carbon@ Cu core–shell nanostructure with nearly full solar spectrum absorption and enhanced solar evaporation efficiency, Journal of Materials Chemistry A, 10 (2022) 9575-9581.

[12] C. Song, M.S. Irshad, Y. Jin, J. Hu, W. Liu, Arabic-dome-inspired hierarchical design for stable and high-efficiency solar-driven seawater desalination, Desalination, 544 (2022) 116125.